Predictions of Ion and Electron Pedestal Temperatures in ITER

T. Onjun
Sirindhorn International Institute of Technology,
Thammasat University, Pathum Thani, 12121, Thailand

Abstract

Models for the prediction of ion and electron pedestal temperatures at the edge of type I ELMy H-mode plasmas are developed. These models are based on theory motivated concepts for pedestal width and pressure gradient. The pedestal pressure gradient is assumed to be limited by high n ballooning mode instabilities, where both the first and second stability limits are considered. The effect of the bootstrap current, which reduces the magnetic shear in the steep pressure gradient region at the edge of the H-mode plasma, can result in access to the second stability mode of ballooning. In these pedestal models, the magnetic shear and safety factor are calculated at one pedestal width away from separatrix. The predictions of these models are compared with the high resolution pedestal data for type I ELMy H-mode discharges obtained from the latest public version (version 3.2) in the International Tokamak Physics Activity Edge (ITPA) Pedestal Database. The predictions of ion and electron pedestal temperatures for ITER using these models are carried out. It is found that at the design point, assuming a flat density profile, the pedestal temperature of ITER is about 2.3 keV.

Keywords: Tokamak, H-mode, Pedestal, Stability

1. Introduction

It is well known that when the plasma heating power increases, plasmas can undergo a spontaneous self-organizing transition from a low confinement mode (L-mode) to a high confinement mode (H-mode). This plasma activity is widely believed to be caused by the generation of a flow shear at the edge of the plasma, which is responsible for suppressed turbulence and transport near the edge of the plasma. The reduction of transport near the plasma edge results in a narrow sharply-defined region at the edge of the plasma with steep temperature and density gradients, called the pedestal. This pedestal is located near the last closed magnetic flux surface and typically extends over with a width of about 5% of the plasma minor radius. It was found that energy confinement in the H-mode regime of tokamaks strongly depends on the temperature and density at the top of the pedestal [1]. Therefore, it is important in H-mode tokamak plasma studies, especially for the burning plasma experiment such as the International Thermonuclear Experimental Reactor (ITER) [2], to have a reliable prediction for temperatures at the top of the pedestal.

In the previous pedestal study by T. Onjun *et al.* [3], six theory-based pedestal temperature models were developed using different models for the pedestal width, together with a ballooning mode pressure gradient limit, that is restricted to the first stability of ballooning modes. These models also include the effects of geometry, bootstrap current, and separatrix, leading to a complicated nonlinear behavior. For the best model, the agreement between the model's predictions and experimental data for pedestal temperature is about 30.8% root mean square error (RMSE) for 533 data points from the International Tokamak Physics Activity Edge (ITPA) Pedestal Database. One weakness of these pedestal temperature models is the assumption that the plasma pedestal is in the first stability regime of ballooning modes. It is well known that in some circumstances such as high plasma shaping and low collisionality, a plasma can gain access to second stability, which can result in a significant increase of edge

pressure gradient and, consequently, pedestal temperature.

In this study, three pedestal width models in Ref. [3] are modified to include the effect of the second stability limit of ballooning modes. The predictions from these pedestal temperature models are to be tested against the latest public version of the pedestal data (Version 3.2), obtained from the ITPA Pedestal Database. This paper is organized in the following way: In Section 2, the pedestal temperature model development is described. In Section 3, the predictions of the pedestal temperature resulting from the models are compared with pedestal temperature experimental data. A simple statistical analysis is used to characterize the agreement of the predictions of each model with experimental data. The development and comparison with experimental data for the pedestal density models are shown. In Section 4, conclusions are presented.

2. H-Mode Pedestal Temperature

In the development of the pedestal temperature models described in Ref. [3], two ingredients are required — pedestal width (Δ) and pressure gradient ($\partial p/\partial r$) — while the pedestal density, n_{ped}, is obtained directly from the experiment. The temperature at the top of the pedestal (T_{ped}) can be estimated as:

$$T_{ped} = \frac{1}{2 n_{ped} k} \left| \frac{\partial p}{\partial r} \right| \Delta \qquad (1)$$

where k is the Boltzmann constant. Six ranges of the pedestal models were developed based on Eq. (1) in Ref. [3]. Note that the notation is described in Table 1. Of these, the following three pedestal temperature models are selected for further development in this work. These pedestal models are the flow shear stabilization pedestal width model [$\Delta=C_w(\rho Rq)^{1/2}$] [3], the magnetic and flow shear stabilization pedestal width model [$\Delta=C_w\rho s^2$] [4], and the normalized poloidal pressure pedestal width model [$\Delta=C_wR(\beta_{\theta,ped})^{1/2}$] [5] , where C_w is the pedestal width constant, ρ is the ion gyro radius, s is the magnetic shear, R is the major radius, q is the safety factor and $\beta_{\theta,ped}$ is the normalized pedestal pressure. These pedestal width models will be used together with an improved pressure gradient model to develop new pedestal temperature models.

For the maximum pressure gradient in the pedestal of type I ELMy H-mode discharges, the pedestal pressure gradient is approximated as the pressure gradient limits of high-n ballooning modes in the short toroidal wavelength limit. The ballooning mode is usually described using the magnetic shear vs. normalized pressure gradient diagram (s-α diagram) [6]. Normally, the calculation of ballooning mode stability is complicated, requiring information about the plasma equilibrium and geometry. A number of different codes have been developed for stability analysis, such as HELENA, MISHKA, and ELITE. In Ref. [3], a scaling of the critical normalized pressure gradient, α_c, was proposed by assuming that the pedestal pressure gradient is restricted to first stability limit of ballooning modes:

$$\alpha_c = 0.4s\left[1+\kappa_{95}^2\left(1+5\delta_{95}^2\right)\right] \qquad (2)$$

where s is the magnetic shear, and κ_{95} and δ_{95} are the elongation and triangularity at the 95% flux surface. However, it has been widely observed in a number of experiments that the pedestal can obtain access to a second stability limit of ballooning mode, especially in high triangularity discharges [7-9]. Here, the scaling of the critical normalized pressure gradient in Eq. (2) is extended to include the effect of second stability of ballooning modes.

In Ref. [10-12], stability analyses for several JET H-mode discharges were carried out using the HELENA and MISHKA ideal MHD stability codes. The results suggest a simple form for the s-α MHD stability diagram as shown in Fig. 1, which leads to an analytic expression for α_c that includes the effect of both the first and second stability of ballooning modes given by:

$$\alpha_c = C_0\alpha_0(s)\left(1+\kappa_{95}^2\left(1+5\delta_{95}^2\right)\right). \qquad (3)$$

where C_0 is a constant and

$$\alpha_0(s)=\begin{cases}3+0.8(s-4) & ;s>4\\ 5-2\sqrt{1-\left(\frac{4-s}{2}\right)^2} & ;4\geq s\geq 2\\ 2.5s & ;s<2\end{cases} \quad (4)$$

The numerical coefficients used in Eq. (4) are chosen according to the stability results computed using the HELENA and MISHKA codes in Ref. [10-12]. It is worth noting that, for $s > 4$, Eq. (4) indicates that the pedestal is in the first stability regime of ballooning modes. For $4 \geq s \geq 2$, the scaling in Eq. (4) represents the regime of a transition from first to second stability of ballooning modes. For $s < 2$, the scaling in Eq. (4) represents a plasma that is in the second stability of ballooning modes, where the pedestal pressure gradient is limited by finite n ballooning mode stability. It is also noted that the effect of the current-driven peeling mode is not considered in this work. In Eq. (4), the bootstrap current and separatrix effects are included through the calculation of magnetic shear as described in Ref. [3].

3. Results and Discussions

Statistical comparisons between the predicted pedestal parameters and corresponding experimental values obtained from the ITPA Pedestal Database [13] version 3.2 are summarized in terms of the RMSE presented in Table 2. The comparison is carried out for the high resolution pedestal data, which consist of 124 data points for the electron pedestal temperature, pedestal width, and pedestal pressure gradient. Note that the definitions of RMSE can be found in Ref. [3]. Results are presented for three pedestal temperature models. These three pedestal temperature models are based on three different models for the pedestal width along with the pressure gradient model for both first and second stability of ballooning modes, where the maximum normalized pressure gradient, α_c, is estimated using Eq. (4). The value of the coefficient, C_w, used in each of the expressions for the pedestal width is given in the second column of Table 2. The value of the coefficient, C_0, used in each of the expressions for the pedestal normalized pressure gradient is given in the third column of Table 2. The values of C_w and C_0 were computed by minimizing the sum RMSE_T_{ped} + RMSE_Δ + RMSE_dp/dr. It is found that the RMSEs for electron pedestal temperature (RMSE_T_{ped}) range from 57% to 63%. For the pedestal width, the RMSEs (RMSE_Δ) range from 30% to 38%. For the pedestal pressure gradient, the RMSEs (RMSE_dp/dr) range from 51% to 56%. All three models yield similar results for the comparison with experiment data.

The comparisons between the predictions of the model based on $\Delta \propto \rho s^2$ and experimental data are shown in Fig. 2 for the pedestal temperature (top panel), the pedestal width (middle panel), and the pedestal pressure gradient (bottom panel). It can be seen that the predictions of pedestal temperature, width and pressure gradient, are in reasonable agreement with experimental data. It is worth showing the improvement of the new pedestal models compared with the previous version of the pedestal models derived in Ref. [1]. Similar comparisons were carried in Ref. [1] using a different database of experimental measurements. Statistical comparisons of the predicted pedestal temperature, pedestal width, and pedestal pressure gradient with experimental data from the new database are shown in Table 2. It can be seen that RMSE_T_{ped} in Tables 2 and 3 are almost the same for all three models, but the RMSE_Δ and RMSE_dp/dr are significantly different.

The effect of using a new pressure gradient model that includes second stability [Eqs. (3) and (4)] can be illustrated by deriving corresponding pedestal models using only the first stability condition [Eq. (2)]. The comparisons between the predictions of the model based on $\Delta \propto \rho s^2$ together with Eq. (2) and experimental data are shown in Fig. 3 for the pedestal temperature (top panel), the pedestal width (middle panel), and the pedestal pressure gradient (bottom panel). It can be seen that the predictions of pedestal temperature are in a reasonable range of experiment, while the pedestal widths are over-predicted and the pressure gradients are under-predicted relative to the data on the average. It can be concluded that the exclusion of access to second stability of ballooning mode results in the under-prediction of the pedestal pressure gradient in most of the discharges. In compensation for the under-prediction of the pedestal pressure gradient, the prediction of the width is over-predicted on the

average in order to maximize agreement with the pedestal temperature.

The pedestal models that include both first and second stability of ballooning mode were derived in this paper using a subset of the database (124 data points) for which pedestal temperature, pedestal width, and pedestal gradient are available. In Table 4, the predictions of these models are compared with the larger number of data points from the full database for the electron pedestal temperature (715 data points) and the ion pedestal temperature (457 data points). Separate models for the ion pedestal temperature are derived by adjusting the value of C_W in order to minimize the RMSE relative to the measured ion temperature values. The models for the electron pedestal temperature remain the same as derived above (in Table 1).

Finally, the pedestal temperature models developed in this paper are used to predict the electron and ion pedestal temperatures for the ITER design. Figure 4 shows the predicted electron pedestal temperature (top panel) and ion pedestal temperature (bottom panel) as a function of pedestal density. It can be seen that the pedestal temperature decreases as the pedestal density increases. At the design point, n_{ped}/n_{gr} =0.84, where n_{ped} is the pedestal density and n_{gr} is the Greenwald density, assuming that the density profile is flat between the magnetic axis and the top of the pedestal. At this point, the pedestal temperature is predicted to be about 2.3 keV. Note that the "design point" would shift to the left in Fig. 4 and, consequently, to a higher pedestal temperature, if the pedestal density were taken to be less than the average plasma density. The predicted results are only slightly different for the ion and electron pedestal temperatures in Fig. 4, as a consequence of the high density in ITER. It is found that the pedestal width in ITER is predicted by all three models to be in the range from 2 to 3 cm. Because of the narrow pedestal width, it is not surprising to obtain relatively low values for the pedestal temperature in ITER.

4. Conclusions

Pedestal temperature models that include the effects of both first and second stability of ballooning modes are developed for type I ELMy H-mode plasmas in tokamaks. The results for the pedestal temperature, width and pressure gradient are compared with high resolution data points in the ITPA Pedestal Database version 3.2. It is found that the inclusion of the second stability of ballooning modes improves the agreement with experimental data for the pedestal pressure gradient and, consequently, for the width. The predictions of ion and electron pedestal temperatures for ITER using these models are carried out. It is found that at the design point with a flat density profile assumption, the pedestal temperature of ITER can reach 2.3 keV.

5. Acknowledgements

T. Onjun is grateful to Dr. Glenn Bateman, Prof. Arnold H. Kritz, and Prof. Suthat Yoksan for helpful discussions and also thanks the ITPA Pedestal Database group for the pedestal data used in this work. This work is supported by Commission on Higher Education and the Thailand Research Fund (TRF) under Contract No. MRG4880165, National Research Council of Thailand, Thailand Toray Science Foundation, and Thammasat University Research Fund.

6. References

[1] Kinsey, J.E., *et al.*, Burning Plasma Projections Using Drift-Wave Transport Models and Scalings for the H-mode Pedestal, Nucl. Fusion, Vol. 43, pp. 1845-1854, 2003

[2] Aymar, R., Barabaschi, P. and Shimomura, Y. (for the ITER team), The ITER Design, Plasma Phys. Control. Fusion, Vol. 44, pp. 519-566, 2002

[3] Onjun, T., *et al.*, Models for the Pedestal Temperature at the Edge of H-mode Tokamak Plasmas, Physics of Plasmas, Vol. 9, pp. 5018-5030. 2002

[4] Sugihara, M., *et al.*, A Model for H-mode Pedestal Width Scaling Using the International Pedestal Database, Nuclear Fusion, Vol. 40, pp. 1743-1756, 2000

[5] Osborne, T.H., *et al.*, H-mode pedestal Characteristics in ITER Shape Discharges on DIII-D, Journal of Nuclear Materials, Vol. 266-269, pp. 131-137, 1999

[6] Wesson, J., Tokamaks, Clarendon Oxford England, 1997

[7] Kamada, Y., *et al.*, Growth of the Edge Pedestal in JT-60U ELMy H-mode, Plasma

Phys. Control. Fusion, Vol. 41, pp. 1371-1378, 1999

[8] Osborne, T.H., *et al.*, The Effect of Plasma Shape on H-mode Pedestal Characteristics on DIII-D, Plasma Phys. Control. Fusion, Vol. 42, pp. A175-A184, 2000

[9] Suttrop, W., *et al.*, Effect of Plasma Shape Variation on ELMs and H-mode Pedestal Properties in ASDEX Upgrade, Plasma Phys. Control. Fusion, Vol. 42, pp. A97-A102, 2000

[10] Onjun, T., *et al.*, Stability Analysis of H-Mode Pedestal and Edge Localized Modes in a Joint European Torus Power Scan, Physics of Plasmas, Vol. 11, pp. 1469-1475, 2004

[11] Onjun, T., *et al.*, Integrated Pedestal and Core Modeling of Joint European Torus (JET) Triangularity Scan Discharges, Phys. Plasmas, Vol. 11, pp. 3006-3014, 2004

[12] Lönnroth, J-S., et al., Integrated Predictive Modelling of the Effect of Neutral Gas Puffing in ELMy H-mode Plasmas, Plasma Phys. Control. Fusion, Vol. 45, pp. 1689-1712, 2003

[13] Hatae, T., *et al.*, Understanding of H mode Pedestal Characteristics Using the Multimachine Pedestal Database, Nucl. Fusion, Vol. 41, pp. 285-294, 2001

Table 1: Notation used in this paper

Symbol	Unit	Description
a	m	Plasma minor radius (half-width)
r	m	Flux surface minor radius (half-width)
R	m	Major radius to geometric center of each flux surface
κ		Plasma elongation
δ		Plasma triangularity
B_T	Tesla	Vacuum toroidal magnetic field at R
I_p	MA	Toroidal plasma current
Mi	AMU	Hydrogenic mass
n_e	m^{-3}	Electron density
T_e	keV	Electron temperature
T_i	keV	Ion temperature
β		Beta $[k_b(n_eT_e+n_iT_i)/(B_T{}^2/2\mu_o)]$
ρ	m	Ion gyroradius
s		Magnetic shear
q		Safety factor

Table 2: Coefficients and RMSEs of the models using the normalized pressure gradient model including both first and second stability limits of ballooning modes.

Width scaling	C_w	C_0	RMSE_T_{ped} (%)	RMSE_Δ (%)	RMSE_dp/dr (%)
$\Delta\propto(\rho Rq)^{1/2}$	0.10	0.8	60	32	56
$\Delta\propto\rho s^2$	0.29	0.8	63	38	51
$\Delta\propto(\beta_{\theta,ped})^{1/2}$	0.012	0.8	57	30	54

Table 3: Coefficients and RMSEs of the models using the normalized pressure gradient model including only first stability limits of ballooning modes.

Width scaling	C_w	RMSE_T_{ped} (%)	RMSE_Δ (%)	RMSE_dp/dr (%)
$\Delta \propto (\rho Rq)^{1/2}$	0.22	57	76	95
$\Delta \propto \rho s^2$	2.41	64	87	96
$\Delta \propto (\beta_{\theta,ped})^{1/2}$	0.021	62	43	81

Table 4: RMSEs of the electron pedestal temperature models using the normalized pressure gradient model including both first and second stability limits of ballooning modes when applied to the full pedestal database.

Width scaling	C_0	Electron pedestal temperature		Ion pedestal temperature	
		C_w	RMSE_T_{ped} (%)	C_w	RMSE_T_{ped} (%)
$\Delta \propto (\rho Rq)^{1/2}$	0.8	0.10	44	0.094	30
$\Delta \propto \rho s^2$	0.8	0.29	37	0.41	31
$\Delta \propto (\beta_{\theta,ped})^{1/2}$	0.8	0.012	167	0.0082	34

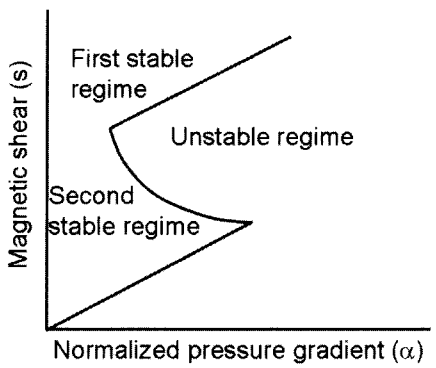

Figure 1: The normalized pressure gradient vs. magnetic shear diagram (s-α diagram) is plotted. First and second stability region and unstable region is also described.

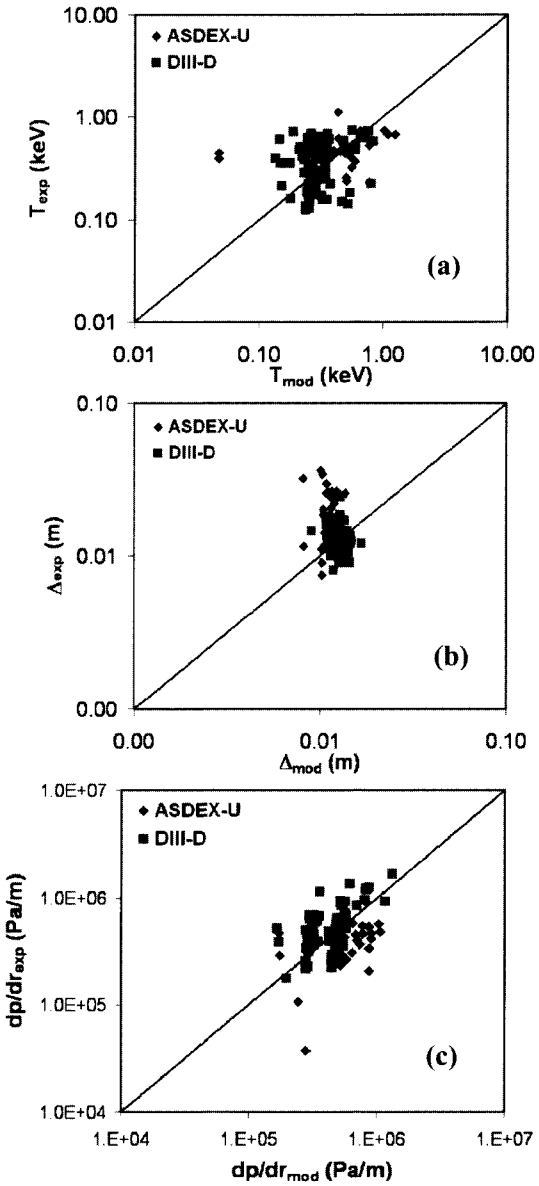

Figure 2: Plot for the pedestal temperature (a), width (b), and pressure gradient (c) predicted by model based on $\Delta \propto \rho s^2$ and the pedestal pressure gradient including both first and second stability of ballooning mode compared with experimental data from 124 data points. Each tokamak is indicated by a different symbol.

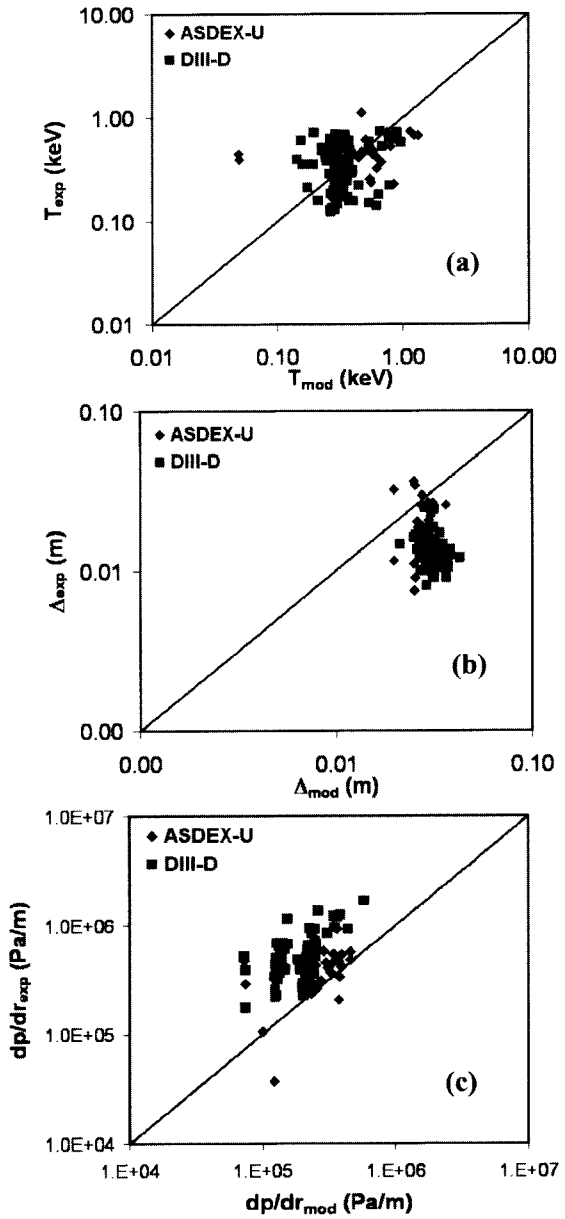

Figure 3: Plot for the pedestal temperature (a), width (b), and pressure gradient (c) predicted by model based on $\Delta \propto \rho s^2$ and the pedestal pressure gradient including only first stability compared with experimental data from 124 data points.

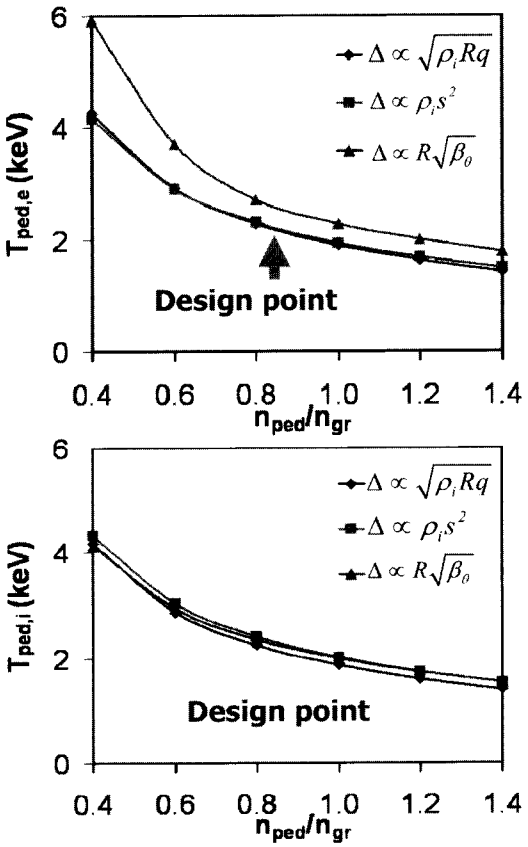

Figure 4: Predictions of electron (top) and ion (bottom) pedestal temperature as a function of the pedestal density based on three pedestal temperature models.